



Cyclopenta[hi]aceanthrylene Decorated with Multiple and Long Alkoxy Chains: Physicochemical Properties and Single-Walled Carbon Nanotubes' Exfoliation Capability

Christoph Schierl,¹ Virtudes Pardo,² Giovanni Bottari,^{2,z} Dirk M. Guldi,^{1,*z} and Tomas Torres^{2,*z}

¹Department of Chemistry and Pharmacy, Interdisciplinary Center for Molecular Materials (ICMM), Friedrich-Alexander-Universität Erlangen-Nürnberg, 91058 Erlangen, Germany

²Departamento de Química Orgánica, Universidad Autónoma de Madrid, 28049 Madrid, Spain

A rod-like cyclopenta[hi]aceanthrylene (CPA) derivative bearing three dodecyloxy chains at each of its two terminal positions was prepared. Spectroscopic (i.e., steady-state absorption and fluorescence) and electrochemical studies carried out with this polycyclic aromatic hydrocarbon (PAH) derivative showed an intense absorption through the entire UV–vis spectral range, weak fluorescence, small HOMO–LUMO gap, and excellent electron accepting capability. Transient absorption spectroscopy (TAS) revealed the formation of singlet and triplet excited states; the latter was, however, only observed in the presence of a triplet sensitizer. The exfoliation capability of this lipophilic CPA towards single-walled carbon nanotubes (SWCNTs) in THF was also investigated. On one hand, transmission electron microscopy (TEM) pointed to an efficient debundling of SWCNTs by the CPA derivative by means of non-covalent interactions. On the other hand, important differences in the ground and excited state features of the uncomplexed and SWCNT-complexed CPA were revealed by Raman and TAS.

© 2020 The Author(s). Published on behalf of The Electrochemical Society by IOP Publishing Limited. This is an open access article distributed under the terms of the Creative Commons Attribution 4.0 License (CC BY, <http://creativecommons.org/licenses/by/4.0/>), which permits unrestricted reuse of the work in any medium, provided the original work is properly cited. [DOI: 10.1149/2162-8777/ab9a5a]



Manuscript submitted May 14, 2020; revised manuscript received May 30, 2020. Published June 22, 2020. *This paper is part of the JSS Focus Issue on Porphyrins, Phthalocyanines, and Supramolecular Assemblies in Honor of Karl M. Kadish.*

Supplementary material for this article is available [online](#)

Fullerenes are carbon caged materials characterized by unique electronic features such as excellent electron affinity, small reorganization energies in electron transfer processes, and good charge transport capabilities.^{1,2} As a consequence of such interesting properties, fullerenes and fullerene derivatives are nowadays among the most widely used *n*-type materials.^{3,4} However, these materials also present some important drawbacks for optoelectronic applications. On one hand, they feature limited absorption across the visible region of the solar spectrum. On the other hand, it is often difficult to fine-tune their HOMO and LUMO energies due to the lack of a resonance effect between the carbon cage and its substituent(s). In the attempt to overcome some of these limitations, the preparation of easy-to-prepare non-fullerene electron acceptors featuring intense solar light absorption and adjustable electronic properties has been pursued.^{5–8} To this end, chromophores such as perylene diimides,⁹ electron-accepting subphthalocyanines,^{10,11} tetracyanobuta-1,3-dienes,^{12–16} or cyclopenta-fused polycyclic aromatic hydrocarbons (CP-PAHs)^{17,18} have been prepared and studied. Among these *n*-type derivatives, CP-PAHs are particularly appealing, with cyclopenta[hi]aceanthrylene (CPA) as one of its most interesting members. CPA is a PAH derivative that, like fullerenes, has an excellent electron affinity,^{19–21} a property arising from pentaannulation, which assists in lowering the CPA LUMO level with respect to non-pentaannulated PAHs.¹⁷ Moreover, CPA presents a planar π -surface, which, upon formation of stacked supramolecular structures, could be potentially beneficial in terms of the material charge transport capability.

To date, several CPA derivatives have been synthesized,^{22–26} in which the electron-accepting CP-PAHs have been connected to electron-donating photo- and electroactive macrocycles,²⁷ incorporated into electron donor-acceptor (D-A) conjugated ladder polymers,²⁸ and copolymers,^{29,30} or mixed with *p*-type polymers into D/A blends.³¹ In the aforementioned studies, the occurrence of photoinduced electron transfer has been demonstrated for the CPA-based conjugates.

Here, we report on the synthesis of a CPA derivative (**1**) functionalized at each of its two terminal positions with three dodecyloxy chains. In particular, the optoelectronic features of **1** were investigated by steady-state and time-resolved spectroscopic techniques, as well as electrochemical measurements, showing an intense and broad absorption, weak fluorescence, small HOMO–LUMO gap, and excellent electron accepting capability. In **1**, the presence of a central planar π -surface and several peripheral long lipophilic chains makes it a perfect candidate to study the exfoliation of single-walled carbon nanotubes (SWCNTs). In this context, an efficient debundling of SWCNTs was observed in THF. Moreover, the formation of **1**/SWCNTs gave rise to an important modification of the ground and excited state features of **1** compared to the uncomplexed derivative.

Experimental

Chemicals were purchased from commercial suppliers and used without further purification unless otherwise stated. Monitoring of the reactions has been carried out by thin layer chromatography (TLC), employing aluminum sheets coated with silica gel type 60 F254 (0.2 mm thick, Merck). Purification and separation of the synthesized compounds were performed by column chromatography, using silica gel (230–400 mesh, 0.040–0.063 mm, Merck). High Resolution Mass Spectrometry (HR-MS) spectra were recorded employing ESI Positive Q-TOF using a Bruker Maxis II, and Matrix Assisted Laser Desorption/Ionization-Time of Flight (MALDI-TOF) using a Bruker Ultraflex III spectrometer, with a Nd:YAG laser. Mass spectrometry data are expressed in *m/z* units. NMR spectra were recorded with a BRUKER AC-400 instrument. The temperature was actively controlled at 298 K. In the ¹H- and ¹³C-NMR spectra, the chemical shifts (δ) are measured in ppm relative to the correspondent deuterated solvent.

CoMoCAT SWCNTs were purchased from Sigma Aldrich.

Steady state absorption spectroscopy was carried out with a Lambda 2 UV/Vis/NIR double beam spectrometer from PERKIN ELMER (190 to 1100 nm). The data was recorded with the software UV WinLab using a slit width of 2 nm and a scan rate of 480 nm min⁻¹. All measurements were performed without

*Electrochemical Society Fellow.

^zE-mail: giovanni.bottari@uam.es; dirk.guldi@fau.de; tomas.torres@uam.es

deaerating in a 10 × 10 mm quartz cuvette (QS) with the respective solvent as reference.

Steady state fluorescence measurements were performed with a FluoroMax[®]-3 fluorometer from HORIBA JOBIN YVON in a 10 × 10 mm Quartz cuvette (QS) without deaerating. All spectra were corrected for the instrument response. Data recording was carried out with the software FluorEssence from HORIBA JOBIN YVON. A slit width of 2 or 4 nm for both excitation and emission as well as an integration time of 0.1 or 0.2 s were applied.

Transient absorption studies in the femto- to microsecond regime were carried out using a transient absorption pump/probe HELIOS/EOS system in combination with an amplified CPA-2110 Ti: sapphire laser (1 kHz, 150 fs pulse width, 775 nm output) from CLARK-MXR Inc. The excitation wavelength at 460 nm was generated with a non-collinear optical parameter (NOPA) from CLARK-MXR Inc. All measurements were conducted in a 2 mm quartz cuvette (OS) under argon atmosphere. The data was recorded with the software HELIOS from Newport/Ultrafast Systems and fitted by multiwavelength (OriginLab, Northampton, MA) as well as global analysis. The latter was performed using the open-source software package GloTarAn, a Java based graphical user interface for the R package TIMP.^{32,33} TIMP is based on spectrottemporal parametrization assuming that the time dependent spectra are linear combinations of different absorption spectra of various species with their respective population profiles.³⁴ An implemented response function accounting for dispersion and the coherent artifact were taken into account.

Electrochemical measurements were recorded with an Autolab PGStat 30 system using a three-electrode configuration system. The measurements were carried out using THF solutions containing 0.1 M of *n*-Bu₄NPF₆. A glassy carbon electrode (3 mm diameter) was used as the working electrode, and a platinum wire and an Ag/AgNO₃ (in CH₃CN) electrode were employed as the counter and the reference electrodes, respectively. Ferrocene (Fc) was added as internal reference and all the potentials were given relative to the Fc/Fc⁺ couple. The scan rate was 100 mV s⁻¹.

Transmission electron microscopy (TEM) was conducted on a Zeiss Leo EM912 Omega with an acceleration voltage of 80 kV.

Raman was performed on WiTec alpha 300r confocal Raman microscope.

Results and Discussion

Synthesis of CPA 1.—CPA derivative **1** was prepared in 33% yield by palladium catalyzed Sonogashira cross-coupling reaction between 2,7-diiodoCPA and 1,2,3-tris(dodecyloxy)-5-ethynylbenzene (Scheme 1).³⁵ CPA derivative **1** as well as its precursors were fully characterized by a wide range of spectroscopic, spectrometric, and electrochemical techniques (see the Supporting Information).

Physicochemical characterization of CPA 1.—We started the physicochemical characterization of CPA derivative **1** with steady state absorption spectroscopy. **1** exhibits absorption features spanning across the entire UV/visible region in toluene (Fig. 1a). For **1**, a

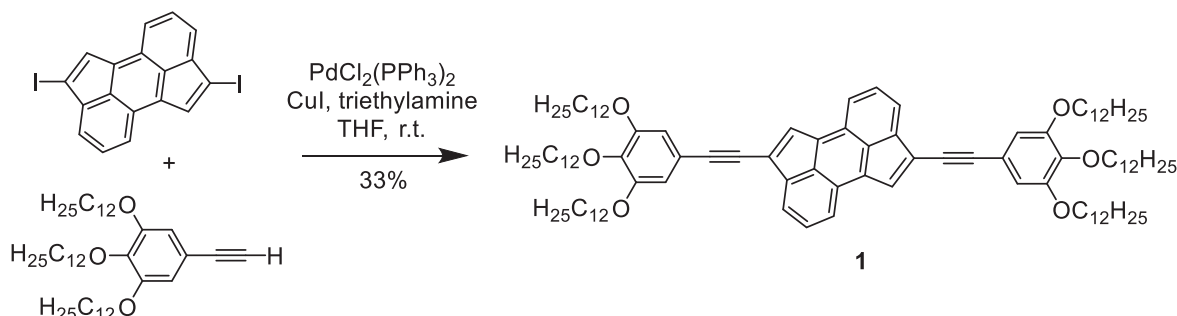
maximum at 321 nm, which is attributable to the peripheral phenyl substituents, was observed followed by a set of well resolved absorptions maximizing at 399, 426, 454, and 481 nm. In contrast, the 550–800 nm region is dominated by a rather broad absorption, to which maxima at 646 and 685 nm are superimposed.

As a complement to steady state absorption spectroscopy, steady state fluorescence measurements on **1** in toluene were performed. Considering the fact that (i) the CPA fluorescence features are broad in nature, and (ii) CPA-centered absorption features extend into the NIR region of the spectrum, the fluorescence detection range was extended beyond 850 nm. For **1**, a fluorescence maximum was observed at around 933 nm (Fig. 1b). Additionally, electrochemical characterization of **1** was carried out by means of cyclic and square wave voltammetry. The corresponding current voltage dependences and the derived potentials in an electrochemical window ranging from -3.0 to +1.5 V are shown in Fig. S2.1 (available online at stacks.iop.org/JSS/9/051011/mmedia) and summarized in Table I. In sound agreement with previous studies on ethynyl-substituted CPA,^{29,36} **1** exhibits the first two reductions at -1.18 and -1.60 V. Notably, the low-lying LUMO energies corroborate the electron accepting nature of the CPA.

Next, we turned to transient absorption measurements. 387 nm excitation of **1** leads to the rapid formation of its singlet excited state features. In THF, these are characterized by minima at 426, 454, 481, 646, and 685 nm, which are due to bleaching of the ground absorption, complemented by maxima at 492, 554, 717, and 1140 nm. The formation of the lowest singlet excited state is completed at time delays of *ca.* 2.6 ps, before it starts to deactivate on the picosecond time scale to yield a full recovery of the ground state (13 ps). Implicit in the aforementioned deactivation is the lack of triplet excited state formation. To bypass the conventional route, that is, intersystem crossing, we focused on triplet-triplet sensitization experiments. In particular, we employed 8.0 × 10⁻⁵ M *N*-methylfulleropyrrolidine (*N*-MFP) in toluene as a triplet sensitizer, which was excited at 387 nm in the presence of **1** in concentration regimes from 0 to 1.0 × 10⁻⁴ M in argon-saturated toluene (Fig. 2a). Following 387 nm excitation, the transient triplet excited state of *N*-MFP—regardless of the concentration of **1**—is formed via a transient singlet excited state by intersystem crossing and gives rise to a characteristic maximum at 700 nm (Fig. 2b). Once the triplet excited state of *N*-MFP is formed, we note the energy transfer to **1** yielding the corresponding triplet excited state markers at 405 and 580 nm, respectively (Fig. 2c). Besides these new maxima, minima at 660 nm evolve in good agreement with the ground state absorption features of **1**. The rate constant for the underlying energy transfer, as it was determined from the CPA concentration dependent decay of the *N*-MFP triplet excited state, is about 4.0 × 10⁹ M⁻¹ s⁻¹.

Table I. Redox potentials of **1** in THF. All values are measured relative to the Fc/Fc⁺ redox couple.

	E ₂ ^{red} /V	E ₁ ^{red} /V	E ₁ ^{ox} /V	E ₂ ^{ox} /V	E ₃ ^{ox} /V	
1	-2.26	-1.60	-1.18	+0.37	+0.63	+0.94



Scheme 1. Synthetic route to CPA derivative **1**.

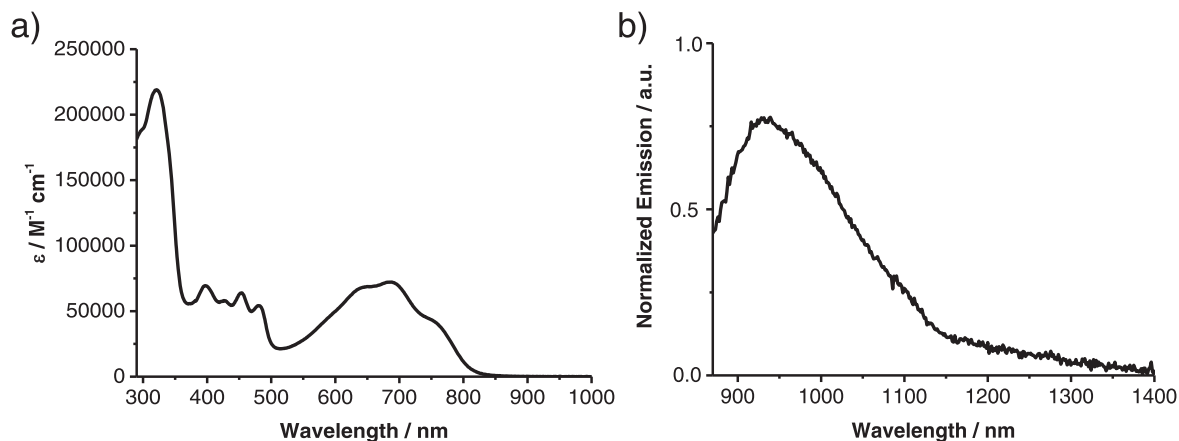


Figure 1. (a) Absorption and (b) fluorescence ($\lambda_{\text{exc}} = 680 \text{ nm}$) spectra of CPA derivative **1** in toluene.

Moreover, an extinction coefficient of $3.3 \times 10^4 \text{ M}^{-1} \text{ cm}^{-1}$ was derived for **1** at 580 nm (Fig. 2d).

Exfoliation capability of CPA 1 towards CoMoCAT SWCNTs.—

The electron accepting behavior of CPA and, in turn, its potential to act as *n*-type material prompted us to implement **1** into a SWCNT-based electron D-A hybrid. To this end, **1**/CoMoCAT SWCNTs were prepared by the sequential enrichment of a solution of **1** in THF with SWCNTs. 0.1 mg of pristine CoMoCAT SWCNTs were added to a $2 \times 10^{-5} \text{ M}$ THF solution of **1** and the resulting suspension was sonicated for 20 min followed by a 10 min centrifugation at 10 kG. Three consecutive enrichment steps were carried out each including addition of CoMoCAT SWCNTs followed by 10 min of sonication and 10 min of centrifugation at 10 kG. For each cycle, the supernatant was separated from the precipitate and used for UV-vis-NIR absorption/NIR fluorescence assays. Absorption and fluorescence spectra

recorded, for example, after three subsequent enrichment steps are displayed in Fig. 3.

The absorption spectrum of pristine CoMoCAT SWCNTs in THF gives rise to typical absorption features of (6,5)-, (7,5)-, and (7,6)-SWCNTs (Fig. 3a, dark line). In particular, S_{22} transitions are found in the visible region of the spectrum at 575 nm for (6,5)-, 658 nm for (7,5)-, and 658 nm for (7,6)-SWCNTs, while the corresponding S_{11} transitions are located in the NIR region with maxima at 1009, 1050, and 1152 nm, respectively.

Upon enrichment of CoMoCAT SWCNTs by CPA **1**, subtle changes in the absorption characteristics relative to **1** and pristine CoMoCAT SWCNTs point towards mutual interactions. As far as **1** is concerned, a marked decrease of the overall absorption intensity goes along with the appearance of a new weak absorption feature around 815 nm (Fig. 3a, grey line). As far as CoMoCAT SWCNTs are concerned, the S_{11} transitions in **1**/SWCNT shift

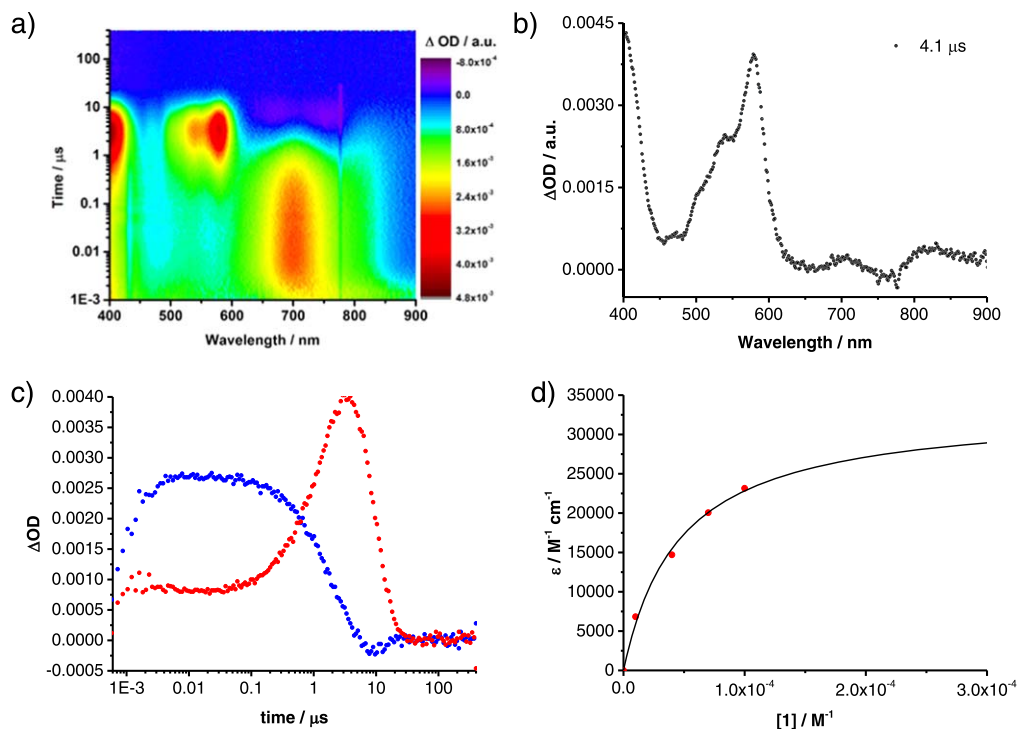


Figure 2. Triplet-triplet sensitization of **1**. (a) Differential absorption changes upon femtosecond pump-probe experiments (387 nm) of N-MFP ($8 \times 10^{-5} \text{ M}$) and **1** ($[1] = 1 \times 10^{-5} \text{ M}$) in argon-saturated toluene with several time delays between 0 and 400 μs . (b) Differential absorption spectra with time delays of 4.1 μs representing the triplet excited state of **1**. (c) Time absorption profiles of the spectra in (a) at 700 nm (blue) and 580 nm (red), illustrating the dynamics of triplet excited state formation of N-MFP followed by transfer of triplet excited state energy to the corresponding triplet excited state of **1**. (d) Plot of the calculated triplet extinction coefficients of **1** vs $[1]$ at 580 nm.

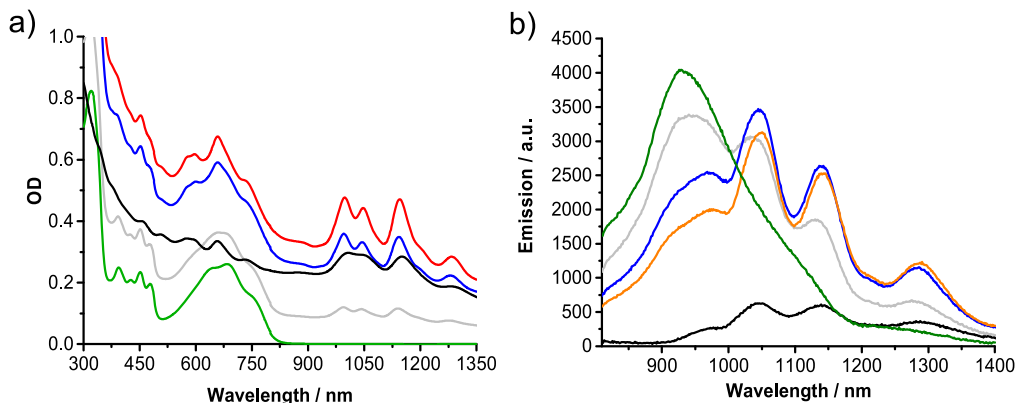


Figure 3. (a) Absorption spectra of CPA **1** (green), pristine CoMoCAT SWCNTs (black), and 1/SWCNTs; the first (grey), second (blue), and third (red) enrichment cycles in THF. (b) Fluorescence spectra following 655 nm excitation of respective solutions/dispersions displayed in the absorption measurements.

hypsochromically by up to 15 nm to 994, 1043, and 1140 nm for (6,5)-, (7,5)-, and (7,6)-SWCNTs, respectively. This contrasts, however, the bathochromic shifts usually observed in case of electronic interactions. In addition, a significant sharpening of the SWCNT-centered absorption features is noted. We attribute the hypsochromic shift and the sharpening to an efficient debundling of SWCNTs induced by interactions with CPA **1**.³⁷ Further confirmation for our interpretation came from titration assays, where **1** was stepwise added to pre-dispersed SWCNTs in THF; sonicated and ultracentrifuged in the absence of **1**. Importantly, without sonicating no substantial sharpening of the absorption features is discernable. Instead, small red shifts of up to 5 nm, for instance, for the (7,6)-SWCNTs are noticeable.

In terms of fluorescence, the 930 nm fluorescence of **1** is gradually quenched throughout the SWCNT enriching steps. For the CoMoCAT SWCNT related fluorescence, no significant quenching is observed (Fig. 3b). The aforementioned debundling of the SWCNTs and, in turn, increased fluorescence, is counter-balanced by the fluorescence quenching caused by electronic interactions with **1**.

An analysis of 1/CoMoCAT SWCNTs by means of Raman spectroscopy was carried out by drop casting THF dispersions of 1/CoMoCAT SWCNTs or CoMoCAT SWCNTs onto gold coated object slides (Fig. 4). All spectra were baseline-corrected and normalized with respect to the G^+ -mode. First, the radial breathing mode (RBM) is considered. In CoMoCAT SWCNT, RBMs are detected at 268, 283, and 311 cm^{-1} , which relate to the (7,6)-, (7,5)-, and (6,5)-SWCNTs, respectively.³⁸ In 1/CoMoCAT SWCNTs, the RBMs appear at 268, 282, and 310 cm^{-1} . They vary, however, slightly in intensities, a trend which leads us to conclude that some kind of chirality selective interactions between **1** and SWCNTs are

operative. Additional insight is gained by a careful analysis of the G^+ -mode, which is shifted from 1591 cm^{-1} in pristine CoMoCAT SWCNTs to 1592 cm^{-1} in 1/CoMoCAT SWCNTs. Shifts in the G^+ -mode are typically seen upon SWCNT doping.³⁹ Upshifts of the G^+ -mode, as seen for 1/CoMoCAT SWCNTs, are in sound agreement with a charge redistribution in SWCNTs upon interactions with **1** and, in turn, a weak but noticeable *p*-type doping.⁴⁰

To complement the spectroscopic investigations of 1/CoMoCAT SWCNTs, TEM was utilized to corroborate the degree of debundling and individualization. Reference experiments were carried out with CoMoCAT SWCNTs in THF. Respective dispersions were drop casted onto lacey carbon supported copper and probed. TEM images of CoMoCAT SWCNTs in THF reveal mainly medium to large sized bundles with average diameters of 5–8 nm and maximal 18 nm next to some smaller bundles of 2 and 4 nm in size. Representative images of 1/CoMoCAT SWCNTs are shown in Fig. 5. Efficient 1/CoMoCAT SWCNTs debundling was discernible throughout the scanned areas. As a matter of fact, the bundle diameter distribution for 1/CoMoCAT SWCNTs is significantly narrowed relative to what was seen for pristine SWCNTs; bundles are much thinner with average diameters between 2 and 3 nm. Considering diameters of about 1.3 nm, the latter reasonably represent the average diameter of the CoMoCAT SWCNTs. Notably, tangling around the lacey carbon grid supports our conclusion as it is commonly observed in highly individualized SWCNT samples.⁴¹

Insights into excited state dynamics of 1/CoMoCAT SWCNTs came from femtosecond pump probe experiments. As a mirror image of the ground state absorption features, differential absorption spectra recorded following 387 nm photoexcitation of CoMoCAT SWCNTs in THF give rise to minima at 575, 598, 658, 740, 1012, 1045, and 1149 nm (Fig. 6). Maxima emerged at 485, 538, 624, and

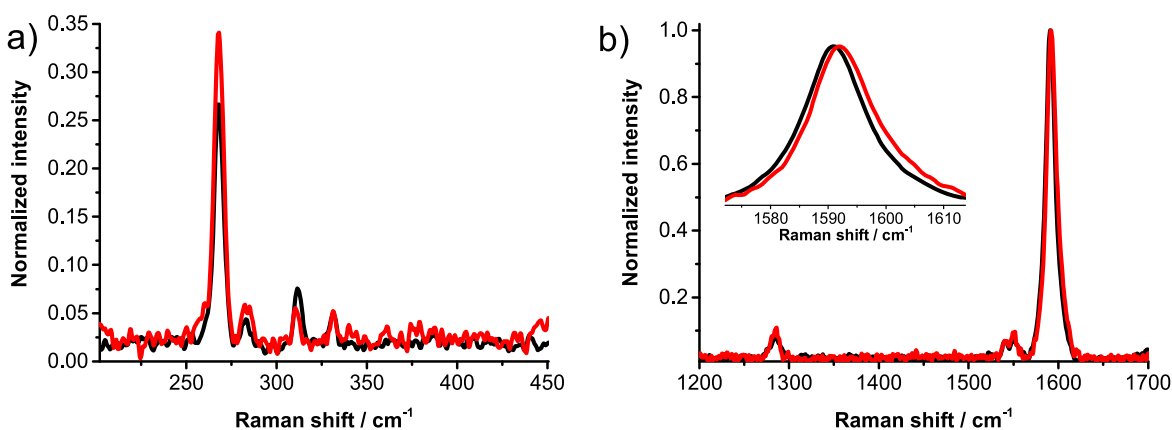


Figure 4. Solid state Raman spectra of SWCNTs (black) and 1/SWCNTs (red) following 1064 nm excitation with focus on (a) RBMs, and (b) D- and G-modes (inset shows a zoom onto the G-mode).

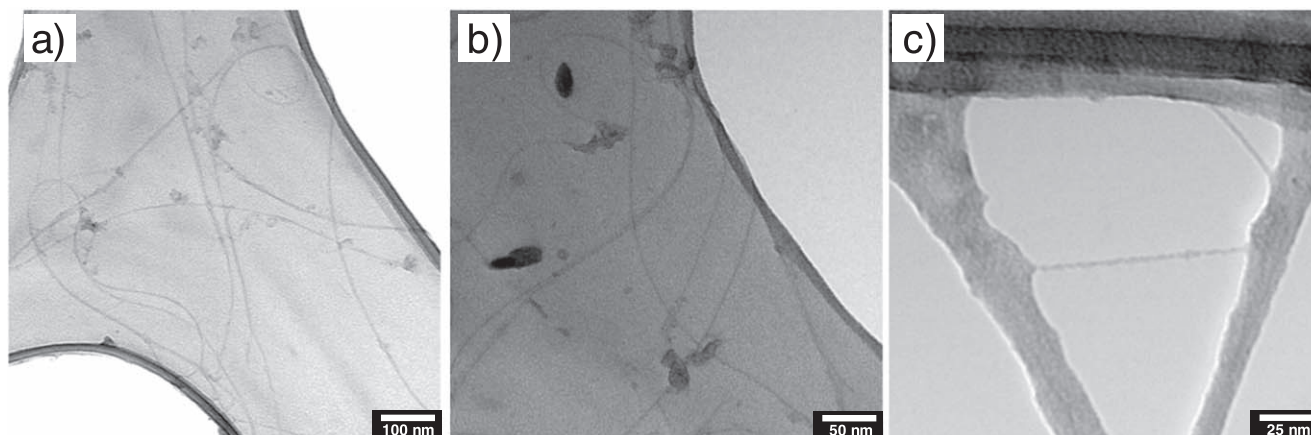


Figure 5. (a)–(c) TEM images of **1**/SWCNTs on lacey carbon grid.

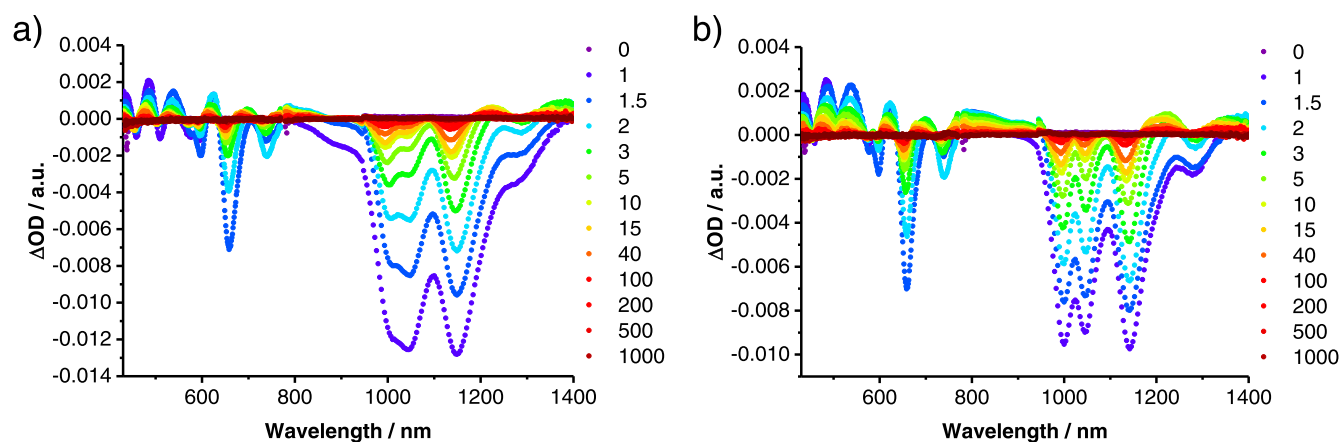


Figure 6. Differential absorption spectra upon femtosecond pump-probe experiments (387 nm) of (a) SWCNTs and (b) **1**/SWCNTs in THF with time delays between 0 and 1000 ps.

697 nm in the visible region as well as at 787, 1224, and 1347 nm in the NIR region of the spectrum. Within the first 40 ps, all of the aforementioned features are subject to noticeable blue shifts due to interband-intertube relaxation and radiative exciton recombination. For instance, the minima shift by as much as 18 nm leading to minima at 994, 1034, and 1135 nm.

For **1**/CoMoCAT SWCNTs, the corresponding minima in THF are located at 575, 598, 659, 739, 999, 1046, and 1144 nm. Upon photoexcitation of **1**/CoMoCAT SWCNTs, slightly blue shifted and well resolved ground state absorption features are noted throughout the early time scales. In addition to the same maxima as in CoMoCAT SWCNTs, a new positive feature at 910 nm is visible. The blue shifts of the transient minima for **1**/CoMoCAT SWCNTs,

which evolve within the first 40 ps, are rather subtle with values that range from 6 to 8 nm.

From the analysis of the excited state kinetics of **1**/CoMoCAT SWCNTs, we conclude a substantial influence of **1** on the SWCNT-centered deactivation (Fig. 7). For both **1**/CoMoCAT SWCNTs and CoMoCAT SWCNTs multiwavelength analyses yield fast and multiexponential decays including three major species. In CoMoCAT SWCNTs, the two shorter lifetimes of 0.9 and 5.7 ps are attributed to radiationless excitonic inter- and intra-band relaxation in bundles, while the longer lifetime of 90.0 ps is associated with radiative inter-band recombination processes.^{42,43} With 0.8, 4.6, and 68.1 ps for **1**/CoMoCAT SWCNTs, we infer an altered excited state deactivation pathway in the presence of **1**.

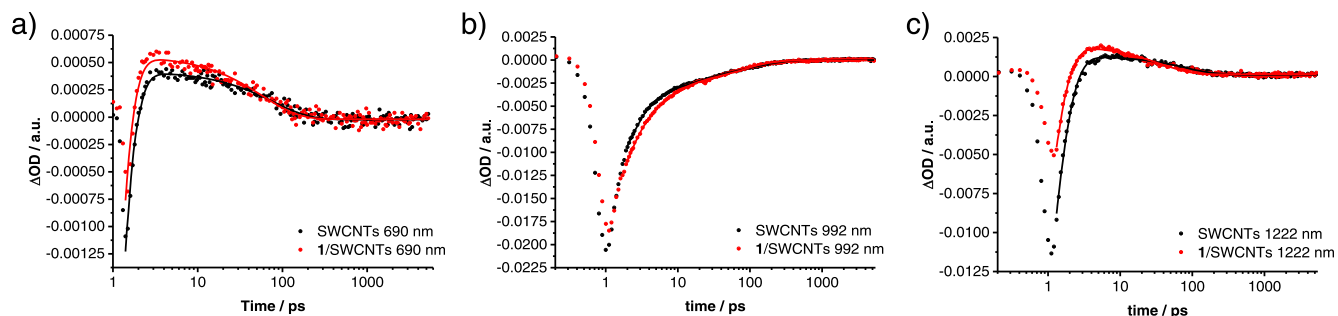


Figure 7. Time absorption profiles of the respective spectra of SWCNTs (black) and **1**/SWCNTs hybrid (red) in THF at (a) 690, (b) 992, and (c) 1222 nm.

Conclusions


In this work, a rod-like CPA derivative (**1**) functionalized at each of its two terminal positions with three dodecyloxy chains has been prepared. In-depth photophysical and electrochemical studies on **1** revealed an intense and broad absorption through the UV–vis region of the solar spectrum, weak fluorescence, small HOMO–LUMO gap, and excellent electron affinity. Additionally, the exfoliation capability of **1** towards SWCNTs in THF were explored, profiting from the presence, in the CPA derivative, of a central planar π -surface and several peripheral long lipophilic chains. Interestingly, an efficient debundling of the SWCNTs by the CPA derivative in THF was observed, accompanied by an important modification of the ground and excited state features of the **1**/SWCNT supramolecular ensemble compared to the uncomplexed derivative.

Acknowledgments

Financial support from the “Solar Energy goes Hybrid” Initiative of the Bavarian Ministry for Science, Culture and Education (SolTech), Comunidad de Madrid (FOTOCARBON), and Spanish MICINN (CTQ2017-85393-P) is acknowledged.

ORCID

Giovanni Bottari  <https://orcid.org/0000-0001-6141-7027>

Dirk M. Guldi  <https://orcid.org/0000-0002-3960-1765>

Tomas Torres  <https://orcid.org/0000-0001-9335-6935>

References

- V. Strauss, A. Roth, M. Sekita, and D. M. Guldi, *Chem.*, **1**, 531 (2016).
- Y. Zhang, I. Murtaza, and H. Meng, *J. Mat. Chem. C*, **6**, 3514 (2018).
- T. L. Nguyen, T. H. Lee, B. Gautam, S. Y. Park, K. Gundogdu, J. Y. Kim, and H. Y. Woo, *Adv. Funct. Mater.*, **27**, 1702474 (2017).
- B. C. Thompson and J. M. J. Frechet, *Angew. Chem. Int. Ed.*, **47**, 58 (2008).
- S. Li, W. Liu, C.-Z. Li, M. Shi, and H. Chen, *Small*, **13**, 1701120 (2017).
- G. Zhang, J. Zhao, P. C. Y. Chow, K. Jiang, J. Zhang, Z. Zhu, J. Zhang, F. Huang, and H. Yan, *Chem. Rev.*, **118**, 3447 (2018).
- E. M. Speller, A. J. Clarke, J. Luke, H. K. H. Lee, J. R. Durrant, N. Li, T. Wang, H. C. Wong, J.-S. Kim, W. C. Tsoi, and Z. Li, *J. Mat. Chem. A*, **7**, 23361 (2019).
- A. Wadsworth, M. Moser, A. Marks, M. S. Little, N. Gasparini, C. J. Brabec, D. Baran, and I. McCulloch, *Chem. Soc. Rev.*, **48**, 1596 (2019).
- N. Zink-Lorre, E. Font-Sanchis, A. Sastre-Santos, and F. Fernandez-Lazaro, *Chem. Commun.*, **56**, 3824 (2020).
- K. Cnops, B. P. Rand, D. Cheyns, B. Verreert, M. A. Empl, and P. Heremans, *Nat. Commun.*, **5**, 3406 (2014).
- G. Zango, T. Sakurai, B. Urone, H. Saeki, W. Matsuda, M. Victoria Martinez-Diaz, S. Seki, and T. Torres, *Chem. Eur. J.*, **24**, 8331 (2018).
- M. Sekita, B. Ballesteros, F. Diederich, D. M. Guldi, G. Bottari, and T. Torres, *Angew. Chem. Int. Ed.*, **55**, 5560 (2016).
- L. M. Urner, M. Sekita, N. Trapp, W. B. Schweizer, M. Wörle, J.-P. Gisselbrecht, C. Boudon, D. M. Guldi, and F. Diederich, *Eur. J. Org. Chem.*, 91 (2015).
- K. A. Winterfeld, G. Lavarda, J. Guilleme, M. Sekita, D. M. Guldi, T. Torres, and G. Bottari, *J. Am. Chem. Soc.*, **139**, 5520 (2017).
- K. A. Winterfeld, G. Lavarda, J. Guilleme, D. M. Guldi, T. Torres, and G. Bottari, *Chem. Sci.*, **10**, 10997 (2019).
- K. A. Winterfeld, G. Lavarda, K. Yoshida, M. J. Bayerlein, K. Kise, T. Tanaka, A. Osuka, D. M. Guldi, T. Torres, and G. Bottari, *J. Am. Chem. Soc.*, **142**, 7920 (2020).
- C. Koper, M. Sarobe, and L. W. Jenneskens, *Phys. Chem. Chem. Phys.*, **6**, 319 (2004).
- A. Modelli, L. Mussoni, and D. Fabbri, *J. Phys. Chem. A*, **110**, 6482 (2006).
- H. Dang, M. Levitus, and M. A. Garcia-Garibay, *J. Am. Chem. Soc.*, **124**, 136 (2002).
- C. Lütke Eversloh, Y. Avlasevich, C. Li, and K. Müllen, *Chem. Eur. J.*, **17**, 12756 (2011).
- X. Zhu, B. Yuan, and K. N. Plunkett, *Tetrahedron Lett.*, **56**, 7105 (2015).
- C.-H. Lee and K. N. Plunkett, *Org. Lett.*, **15**, 1202 (2013).
- S. R. Bheemireddy, P. C. Ubaldo, P. W. Rose, A. D. Finke, J. Zhuang, L. Wang, and K. N. Plunkett, *Angew. Chem. Int. Ed.*, **54**, 15762 (2015).
- S. R. Bheemireddy, P. C. Ubaldo, A. D. Finke, L. Wang, and K. N. Plunkett, *J. Mat. Chem. C*, **4**, 3963 (2016).
- S. R. Bheemireddy, P. C. Ubaldo, P. W. Rose, A. D. Finke, J. Zhuang, L. Wang, and K. N. Plunkett, *Angew. Chem. Int. Ed.*, **54**, 14140 (2015).
- A. R. Mohebbi and F. Wudl, *Chem. Eur. J.*, **17**, 2642 (2011).
- C. Schierl, W. Alex, L. M. Mateo, B. Ballesteros, D. Shimizu, A. Osuka, T. Torres, D. M. Guldi, and G. Bottari, *Angew. Chem. Int. Ed.*, **58**, 14644 (2019).
- S. R. Bheemireddy, M. P. Hautzinger, T. Li, B. Lee, and K. N. Plunkett, *J. Am. Chem. Soc.*, **139**, 5801 (2017).
- J. L. Jellison, C.-H. Lee, X. Zhu, J. D. Wood, and K. N. Plunkett, *Angew. Chem. Int. Ed.*, **51**, 12321 (2012).
- X. Zhu, J. Yuen, J. Fan, C. Munoz, M. F. Wang, R. S. Shirazi, J. Seifert, and F. Wudl, *Adv. Mater.*, **23**, 4644 (2011).
- J. D. Wood, J. L. Jellison, A. D. Finke, L. Wang, and K. N. Plunkett, *J. Am. Chem. Soc.*, **134**, 15783 (2012).
- J. J. Snellenburg, S. Laptinok, R. Seger, K. M. Mullen, and I. H. M. van Stokkum, *J. Stat. Soft.*, **49**, 1 (2012).
- K. M. Mullen and I. H. M. van Stokkum, *J. Stat. Soft.*, **18**, 1 (2007).
- I. H. M. van Stokkum, D. S. Larsen, and R. van Grondelle, *Biochim. Biophys. Acta*, **1657**, 82 (2004).
- J. Wu, M. D. Watson, L. Zhang, Z. Wang, and K. Müllen, *J. Am. Chem. Soc.*, **126**, 177 (2004).
- H. Xia, D. Liu, X. Xu, and Q. Miao, *Chem. Commun.*, **49**, 4301 (2013).
- Notably, no absorption changes in the SWCNT features were observed when using a CPA derivative lacking the peripheral 1,2,3-tris(dodecyloxy) chains (i.e., 2,7-bis(trimethylsilyl)ethynyl)CPA instead of **1** suggesting inefficient debundling of the former CPA derivative towards SWCNTs.
- S. M. Bachilo, M. S. Strano, C. Kittrell, R. H. Hauge, R. E. Smalley, and R. B. Weisman, *Science*, **298**, 2361 (2002).
- M. S. Dresselhaus, G. Dresselhaus, R. Saito, and A. Jorio, *Phys. Rep.*, **409**, 47 (2005).
- C. Ehli, C. Oelsner, D. M. Guldi, A. Mateo-Alonso, M. Prato, C. Schmidt, C. Backes, F. Hauke, and A. Hirsch, *Nat. Chem.*, **1**, 243 (2009).
- V. Strauß, A. Gallego, G. de la Torre, T. W. Chamberlain, A. N. Khlobystov, T. Torres, and D. M. Guldi, *Faraday Discuss.*, **172**, 61 (2014).
- J. Kono, G. N. Ostojic, S. Zaric, M. S. Strano, V. C. Moore, J. Shaver, R. H. Hauge, and R. E. Smalley, *Appl. Phys. A*, **78**, 1093 (2004).
- L. Huang, H. N. Pedrosa, and T. D. Krauss, *Phys. Rev. Lett.*, **93**, 017403 (2004).